



An efficient combination of quadruple biomarkers in binary classification using ensemble machine learning technique for early onset of Alzheimer disease

Rashmi Kumari¹ · Akriti Nigam¹ · Shashank Pushkar¹

Received: 7 July 2021 / Accepted: 14 February 2022 / Published online: 8 March 2022
© The Author(s), under exclusive licence to Springer-Verlag London Ltd., part of Springer Nature 2022

Abstract

Background Alzheimer's disease (AD) is a degenerated condition of the brain where memory loss is fully depleted for elderly individual. Efficient machine learning methods are accessible, producing low classification accuracy since single modality features are being evaluated. In this paper, the multimodal approach is developed and execution of comprehensive validation for structural atrophy through Magnetic Resonance Imaging decreases metabolism through Fluorodeoxyglucose Positron Emission Tomography (FDG-PET), and accumulation of amyloid plaques through Pittsburgh compound B (PiB-PET), as well as cognitive assessment for identifying the early onset of AD. It has been stated that additional information from multiple image modalities would ameliorate the classification accuracy while diagnosing early AD. The novel classifier, Adaptive Hyperparameter Tuning Random Forest Ensemble Classifier (HPT-RFE), is proposed for three binary classifications. In this classifier, the tuning of hyperparameters is automated for computing the best features while constructing the optimum size of Random Forest. The advantage of using the classifier is computationally much faster when compared with Support Vector Machine, Naïve Bayes, K-Nearest Neighbour and Artificial Neural Network. Simulation results show that the performance of the Adaptive HPT-RFE classifier has been regarded as best among all binary classifications in the ADNI dataset. For AD versus Normal Control (NC) binary classification, 100% accuracy, sensitivity, and specificity have been achieved, whereas the accuracy of 91% and 100% specificity for NC versus Mild Cognitive Impairment (MCI) classification and 95% accuracy, 100% specificity, 80% sensitivity for AD versus MCI classification are compared with four state-of-the-art techniques.

Keywords Alzheimer disease · Magnetic resonance imaging · Fluorodeoxyglucose · Pittsburgh compound B · Positron emission tomography · High performance computing · FreeSurfer

1 Introduction

One of the global challenges in the health care industry is AD, affecting more than 5 million American people [1]. Due to adverse complications in AD, it has been predicted that more than 7 million people died aging more than 65 years [2]. The cases of AD patients would be double every five years after attaining the age of 65 years. In addition to that, AD is almost one-third of the total population aging more than 85 years [3]. For memory disability

and other cognitive problems, the characterization of AD is exhibited by neurofibrillary entanglement [4, 5]. For an association in the memory losses in AD patients, molecular mechanisms are still unknown. Some healthy individuals do not have memory loss but possessing plaques and deposits [6]. Risk factors such as obesity, age, diabetics, and inflammation increment in the brain occurred in AD [7]. *APOE* is the most vital supplementary risk factor among *CRI*, *FERMT2*, and *COMT* genotypes [8]. According to the National Institute of Aging and the Alzheimer's Disease Association, preclinical AD, MCI, and dementia are the three stages of AD [9]. Encephalopathy or cognitive impairment occurs at the first stage (preclinical) AD. The primary cause of AD is dementia which encompasses mild, moderate, and severe phases. Amyloid

✉ Rashmi Kumari
phdcs10064.17@bitmesra.ac.in

¹ Department of CSE, BIT Mesra, Ranchi, India

positivity, Asymptomatic cerebral amyloidosis [10], synaptic dysfunction are the divisions of Preclinical AD. Declining of cognitive functions and neurodegeneration are shreds of evidence found in all three divisions. Clinical diagnosis, the background of the disease, psychological tests with additional information are some of the methods in diagnosing AD. To assist AD, non-protruding eye tests are being conducted. In addition to that, an association of beta-amyloid protein present in the eye has significant roles in the levels of the brain [11]. Neuroimaging method poses a crucial part of evaluating suspected AD patients. The two other modalities for diagnosing AD are PET and MRI. Brain's structural and functional information is acquired through MRI using the detailed characterization of tissues with a difference in soft tissues. This technique can easily differentiate white matter and grey matter where brain tissues are displayed. Molecular and metabolic information of the brain is obtained by PET imaging which is not restrained to A β and glucose. High sensitivity is achieved for the distribution of tangles and plaque lesions in AD patients. As a result, this modality helps to diagnose normal and different stages of AD qualitatively and quantitatively [12]. Hence, combined imaging techniques of MRI and PET would facilitate diagnosing AD other than any other technique. In the last few decades, the application of hybrid imaging models is gaining importance in the clinical fields. Some of the models include PET/Computed Tomography (CT), single-photon emission computed tomography (SPECT), and fluorescence molecular tomography (FMT). In radiation areas, the PET/MR hybrid imaging model is applied to AD patients for better performance [13]. For correction in attenuation of soft tissues, Dixon MR produces satisfactory results and is applicable in FDG uptakes to identify lesions in brain tissues. Hence, PET/MR imaging model finds its potential application in the areas such as classification, different stages of the disease, diagnostic evaluation, and comprehension of pathomechanisms [14]. In addition to that, a single imaging session produces all imaging and biomarkers information that assists patients and referred physicians [12].

Previous studies show that there has been a remarkable increase in retention of PiB Biomarker, which is observed as elevated plaques levels comparing with HC subjects. PiB patterns produce retention in parietal and frontal cortices of brain regions, which is entirely different for AD patients [15]. In cortical areas of AD patients, PiB retention has been considered most prominent, whereas lowest in areas of white region processing the studies related to a post-mortem of A β plaques [16]. In AD's frontal, temporal, parietal cortex of the brain, retention of PiB has been observed. Significantly affected areas in the brain's occipital and lateral temporal cortex have prudently been observed in mesial temporal regions. In the previous

studies relating extensive A β deposition, retention of striatal PiB has been significantly observed in AD striatum patients [17]. Hence, the description of A β deposition is mentioned and confirmed by using PiB in AD and CN subjects [18]. The main highlights of the paper are as follows:

1. In this study, multimodal approach is developed for comprehensive validation in structural atrophy through MRI, decrease metabolism through FDG-PET and accumulation of amyloid plaques through PiB-PET as well as cognitive assessment for studying early patterns for diagnosing AD.
2. FreeSurfer 6.0.1 has been applied in MRI, FDG-PET and PiB-PET images for extracting different features, such as morphometric features, Region of Interest (ROI), Surface features, Standard Uptake Values (SUV) and cognitive assessment in High Performance Computing (HPC).
3. Adaptive HPT-RFE classifier is based on one versus one classification which leads to three binary classification, namely AD versus NC, MCI versus NC and AD versus MCI and compared with SVM, NB, KNN, and ANN classifiers which makes model a robust and stable one.
4. The performance of Adaptive HPT-RFE classifier has been applied on 102 subjects which has been taken from Alzheimer's disease Neuroimaging Initiative (ADNI) database and compared with other four state-of-the-art techniques in each binary classification tasks where simulation results indicate that model has a good potential for generalisation.

The paper's organization is as follows: Sect. 2 describes the related works. Sect. 3 describes methods. Section 4 illustrates Image Processing. Classification methods are discussed in Sect. 5. Simulation results and discussions are presented in Sect. 6. Finally, the conclusion of the proposed study is explained in Sect. 7.

2 Related works

There has been no concrete treatment for AD where modern therapies are modified to degrade the progression of the disease. The main criteria of conducting trials are to measure cognitive functions by applying ADAS-cog [19] and CDR Scale [20]. It has been observed that clinical symptoms of patients vary according to the progression of AD. This disease does not closely correlate with beta-amyloid (A β) proteins and tau deposition with losses [21]. Applying ADAS-Cog psychometric tests [22] and brain cognitive reserve capacity [23], modification of clinical symptoms is well presented. Therefore, biomarkers are

used for assessing the effectiveness of the disease in convenient histopathological features of AD [24]. Biomarkers, such as 11C- PiB, are applied in cerebrospinal fluid (CSF) for predicting accumulation of A β 1–42 [21]. CSF p-tau and tau PET are the two biomarkers used in tau pathology. Biomarkers, such as PET, take uptake values for specific regions in FDG, MRI for neuronal loss atrophy, and CSF in elevated t-tau protein [21]. Most biomarkers are investigated for clinical symptoms by calculating the following parameters: specificity, validity, transition, and correlation with other biomarkers [25]. For the same patient, rare studies are conducted at many time intervals for more than two biomarkers, and all biomarkers are not readily available for all subjects.

Amyloid or tau PET are popular imaging methods for treating patients having dementia about complaints in cognitive functions induced by changes in neurodegenerative. Interdependence between aspects of pathology and physiology are investigated. Different studies are conducted, which shows that experimental analysis of imaging methods is becoming potential for evaluating pathophysiologic changes. For observing the dynamic changes in the brain, conventional imaging methods such as CT and MRI are applied for cognitive impairment. In the neuropsychiatric field, PET/MRI hybrid brain imaging system has been developed, which is beneficent to assess the changes in the cerebral pathophysiological [26]. Hence, this hybrid brain imaging system helps diagnose cerebrovascular diseases and AD [27]. Several research works illustrate the relationships between functional or morphological MRI information and change inflow of blood or metabolism. But limited studies are conducted on integrated analysis of functional MRI and amyloid/tau imaging.

3 Methods

In the proposed framework, there are two processing steps: (1) Pre-processing of images: From the grey matter segmentation of the brain, different sizes of patches are obtained where each feature is extracted from MRI, FDG-PET, and PiB-PET images (2) Classification: Train an HPT-RFE classifier to learn the patterns and discriminate AD, MCI, and NC individuals and applied for three binary classifications.

3.1 Materials

3.1.1 Preparation of dataset

In 2003, the ADNI dataset [28] was created by M.W. Weiner as a public–private partnership for researchers worldwide. The critical ingredient of ADNI is to measure

the progression of MCI to early AD by biomarkers such as MRI, PET, neuropsychological and clinical assessment.

In validating our proposed method, T1WI MRI scans, PiB PET, FDG PET images, and cognitive assessments of 102 ADNI subjects have been used in the study. These subjects have been divided into three cohorts at the time of preparing the manuscript. (1) NC: 11 Male and 8 Female subjects are diagnosed for all points (2) MCI: 44 Male and 21 Female subjects are evaluated for more than two years. (3) AD: 18 subjects are considered with a clinical diagnosis. Here, cognitive assessments of all subjects such as MMSE, GDSCALE, Global CDR, and FAQ scores are displayed in Table 1. In the second row, the numbers in the bracket mention the total number of male and female subjects. In contrast, the rest five rows indicate the two numbers, i.e., minimum and maximum values of parameters used in cognitive assessment. In addition to that, over 4100 MRI images, more than 500 FDG-PET images, and 223 PiB-PET images are applied in categorizing into three cohorts. Procedures of image processing protocols, post-acquisition pre-processing, and comprehensive ADNI cohort are described [29].

3.1.2 MRI protocol

All T1 Weighted 3D MRI (T1WI) Protocol are acquired from SAGITTAL Acquisition Plane, 3D Acquisition Type, 8HRBRAIN Coil, 1.5 Tesla Magnetic Strength, 8 Flip Angle, GE MEDICAL SYSTEMS Manufacturer, 256 pixels of Matrix X and Matrix Y, 166 Pixels of Matrix Z, SIGNA HDx Manufacturer Model, 0.9 mm of Pixel Spacing X and Y, RM Pulse Sequence, 1.2 mm of Slice thickness, 3.8 TE ms, 1000 TI ms, 8.6 TR ms [30].

3.1.3 FDG-PET protocol

All glucose metabolism 3D FDG-PET are acquired from 0.096000 cm⁻¹ Attenuation, Rectangle: 4.300000 mm Ax, rectangle 6.500000 mm Rad Convolution Kernel, EMISSION Counts Source, START Decay Correction, 6 Frames, GE MEDICAL SYSTEMS Manufacturer, Discovery RX Mfg Model, 128.0 pixels of number of rows and columns, 47 Slices, 2 mm of X and Y Pixel Spacing, F-18 Radioisotope, 18F-FDG Radiopharmaceutical, RTSUB Randoms Correction, 3D Kinahan–Rogers Reconstruction, Model-Based Scatter Correction, 3.3 mm Thickness [31].

3.1.4 PiB-PET protocol

All amyloid 3D 11C PiB-PET are acquired from ramp Convolution Kernel, and Dynamic EMISSION Counts Source, START Decay Correction, 27 frames, Siemens/CTI Manufacturer, HR + Manufacturer Model, 128.0

Table 1 Demographic Cohorts, cognitive assessments and participants information: Except the count written in the brackets (Male/Female), Age (in years), MMSE, GDSCALE, Global CDR, FAQ scores are displayed in Mean (Minimum–Maximum) format

	NC	MCI	AD
<i>Count (M/F)</i>			
No. of subjects	19(11/8)	65(44/21)	18(11/7)
No. of MRI Images	922(580/342)	2795(1883/192)	465(289/176)
No. of FDG PET Images	106(65/41)	384(261/123)	59(36/23)
No. of PiB PET Images	49(28/21)	142(94/48)	32(19/13)
<i>Mean (Min–Max)</i>			
Age (in years)	80.5(70.2–93.2)	76.8(55.2–92.6)	73.6(55.2–87.9)
MMSE	28.18(24–30)	25.6(13–30)	20.5(9–26)
GDSCALE	1.17(0–3.5)	2.12(0–11)	1.6(0–8)
Global CDR	0.03(-0.5–0.5)	0.18(0–3)	0.33(0.5–2)
FAQ	3.04(0–9.5)	6.9(0–30)	12.6(0–30)

pixels of the number of rows and columns, 63 Slices, 2.1 mm of *X* and *Y* Pixel Spacing, C-11 Radioisotope, ¹¹C PiB PET Radiopharmaceutical, CPU iterative Reconstruction, Simulated 3D Scatter Correction, 2.4 mm Thickness [32].

3.1.5 FreeSurfer

Nowadays, the primarily used software in VolBM is FreeSurfer (surfer.nmr.mgh.harvard.edu), where complicated image processing operations are implemented [33]. FreeSurfer calculates the corresponding volumes and a massive number of anatomical structures from the segmentation of incoming scans. Here, FreeSurfer version 6.0.1 has been applied in the hippocampus, total GM, temporal GM, and ventricular volume output as an imaging biomarker for the AD brain. Computational complexity is a significant hindrance for FreeSurfer as compared to HPC for limited application in clinical routines. Time taken for the FreeSurfer pipeline for an up-to-date Single processor PC takes 6 to 24 h to complete each scan. A clustering network is used in HPC, composed of 2 Master and Computer Node, 1 GPU Computer Node, and 1 Cloud Node as explained in Fig. 2.

3.1.6 HPC

The HPC configurations [34] are as follows: 2 numbers of Master node and Computer Node of E5-2630 v3 Intel Xeon 2.4 GHz processors with 8-core, Hard Disk Capacity of 500 GB; 1 GPU Compute Node of 2 numbers of Nvidia K20 GPU and 64 GB memory; 1 Cloud node of E5-2620 V3@2.4, 6 core processors E5-2620 and 64 GB Memory, Hard Disk Drive of 1 TB. The overview of cluster network is shown in Fig. 1.

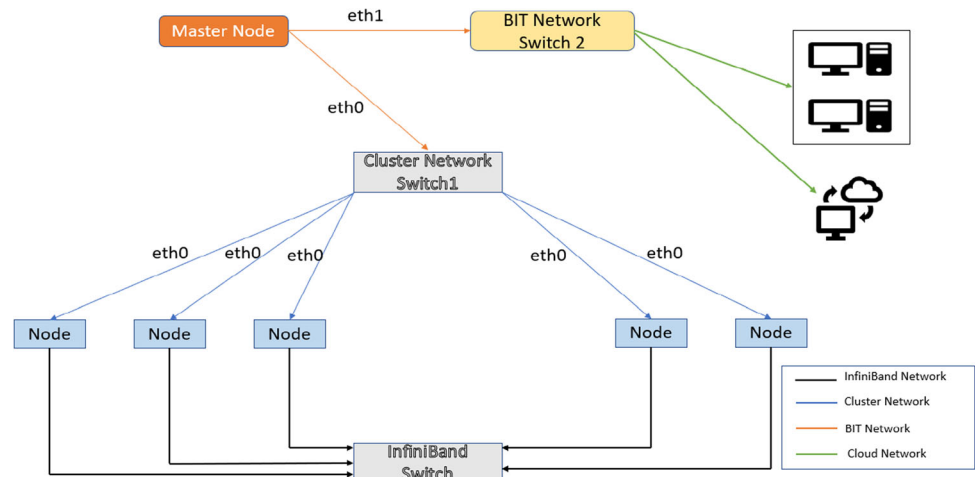
4 Image processing

Due to parameters, such as similar pose, scale, and less heterogeneity along with FDG-PET, PiB-PET, and T1WI MRI images, a small database of images has been acquired from the ADNI dataset. By applying machine learning techniques, high classification accuracy has been achieved. Hence, Voxel-Based Morphometry (VBM), Region of Interest (ROI), Positron Emission Tomography Partial Volume Correction (PET PVC), FDG and PiB features and Standard Uptake Values (SUV) are shown in Fig. 2.

4.1 VBM

It is a neuroimaging analysis method for investigating differences in the brain's focal anatomy by applying statistical tools. To identify the difference in the brain structure and perform quantitative measurements, morphometry analysis has to become a vital tool for research. The main advantage of using the VBM method is to produce an unbiased score that can represent differences created by the brain's anatomical structure [35]. For VBM, 3D volumetric T1WI MRI images are provided. Using various statistical tools, VBM tests all the voxel-based images in the brain. For instance, t tests are performed on each image's voxel for recognizing the pattern differences between two subject groups. In addition to that, measurements of MRI in brain atrophy marked the tracking of AD's progression. A large number of literature reviews related to VBM are studied [36] VBM is applied for studying the volumetric atrophy of grey matter located in the brain's neocortex. The criteria for selecting brain structures are to classify volumes during AD's early or advanced stage [37]. In total, 22 volume features are extracted from the 3D T1WI Global MRI measure of Volume (called subject/stats/ aseg. stats). Four best features are selected by normalization of brain features and ventricular volumes. Figure 3 shows the volume and

Fig. 1 Overview of cluster network



intensity structure-wise FS segmentation. Also, characteristics of Volume are mentioned in Table 3.

4.2 Region of interest (ROI)

3D grey level volume for various brain structures is extracted from 102 subjects [38, 39]. 1 mm³ resolution is required in high-quality T1WI MRI images for pre-processing using FreeSurfer Software. By entering the command “recon-all-I file-name. nii-all”, FreeSurfer Software is executed without the intervention of anyone. This software is used as a process mode for pipelining the preprogrammed processing of the patient’s data. By applying the default parameters, a total of 110 features of Cortical and subcortical volume (Fig. 3) are computed. During the process, Bilateral ROIs are obtained. Between WM, cortical WM, and pial surfaces, FreeSurfer develops a model in the cortical surface stream (Fig. 3). An array of anatomical features such as CTH, curvature, folding, surface normal and area calculations are computed for every cortex part. Desikan-Killiany atlas is adopted for our study, which is applied to 68 labelled regions of the cortex area. In segmenting the automated subcortical regions of the brain, 40 labels are assigned for representing 40 subcortical regions. For each subject, approximately 12 h are required for completing the segmentation of subcortical volume. Table 2 lists the features extracted from T1WI MRI images.

4.3 PET partial volume correction (PVC)

A comprehensive automatic pipelining PET data analysis is executed on the brain’s cortical surface in this study. For PVC, PET Surfer software provides a required number of tools. Applying the *spmregister* tool from FreeSurfer 6.0.1, the registration of PET images to T1 images is the primary step of executing the pipeline. The intensities of PET

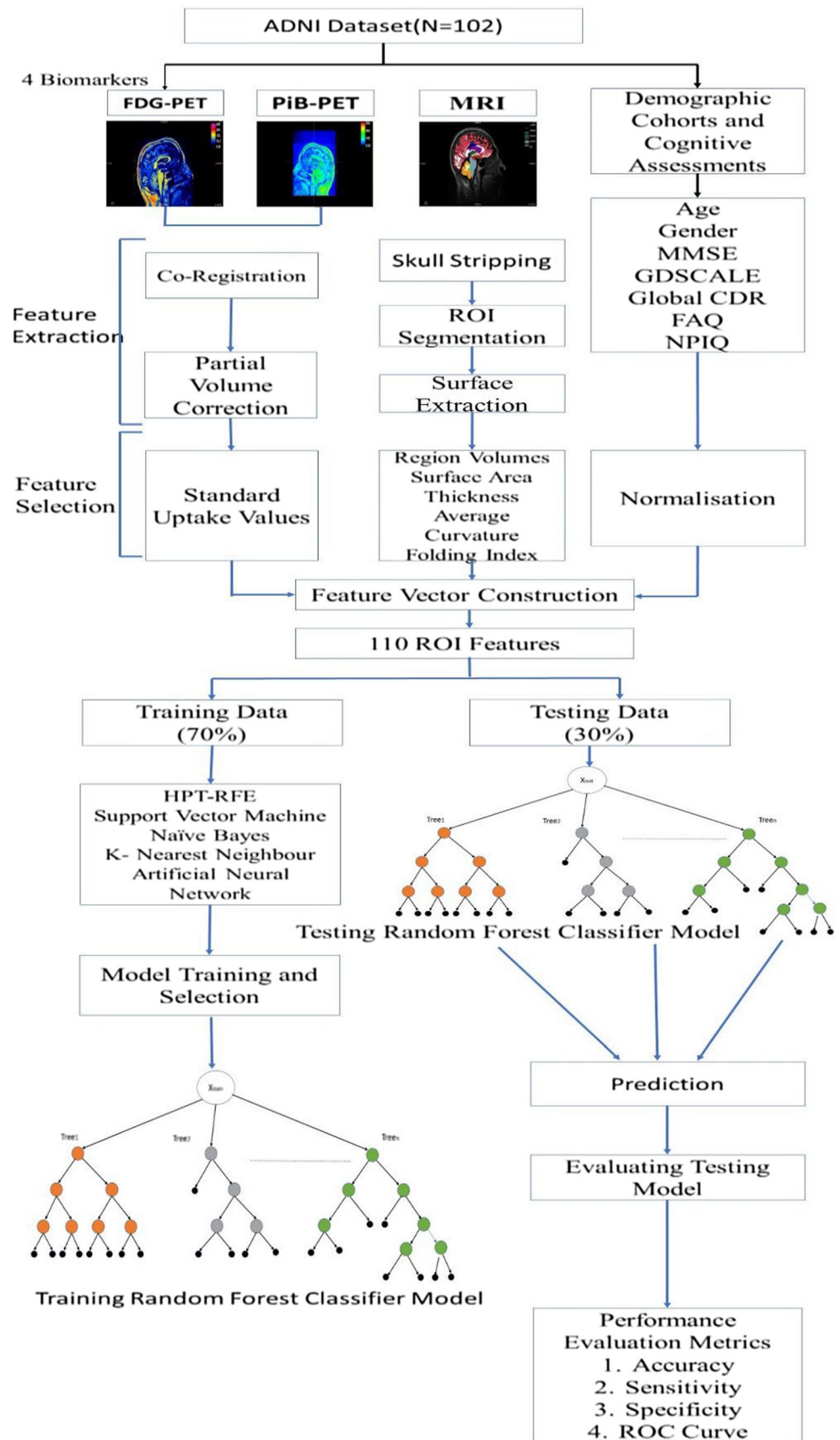
images are normalized for comparing inter subjects. The MNI space pick atlas generated values of SUVs by dividing PET images considering mean uptake values from the reference region [40]. Here, the reference region is taken to be Pons for FDG-PET images [41]. By applying SPM 12, MNI space registration is performed. At first, estimating the transformation to MNI template from T1 and applying inverse deformation in the reference region. 6-mm sphere is eroded for masking of pons so that voxels are considered only within the pons while computing mean uptake. For restricting the outside cortex’s spill-out activity, PVC is performed. In calculating the better computational efficiency, the iterative Yang algorithm [42] has been applied to PET-PVC [43]. In this algorithm, the VOI method is used in which uniform activity within the region is assumed, and parcellated T1 image is obtained. From Freesurfer, the *gmsseg* tool has been applied to parcellated the T1 image of the subject into 112 areas. Suggestions made by the developer of PET-PVC, the fusion of certain regions, are fused to decrease the number to 50. Applying the *mrisc_preproc* tool, the standard template is constructed for each subjects’ cortical surface, where spherical registration is performed [44]. SUVr values are measured, and images are normalized using a template and atlas.

SUVr is defined as the ratio of the concentration of radioactivity *CPET(T)* (kBq/mL) to injection dose administered (MBq) at the same time by the weight of the body (Kg), which is given by formula

$$SUV_{BW} = \frac{C_{PET}(T)}{\frac{Dose}{Weight}} \tag{1}$$

The Pipeline process of PET-PVC is shown in Fig. 4.

Fig. 2 Workflow of proposed methodology in three binary classifications for extracting features from MRI, FDG-PET and PiB-PET images



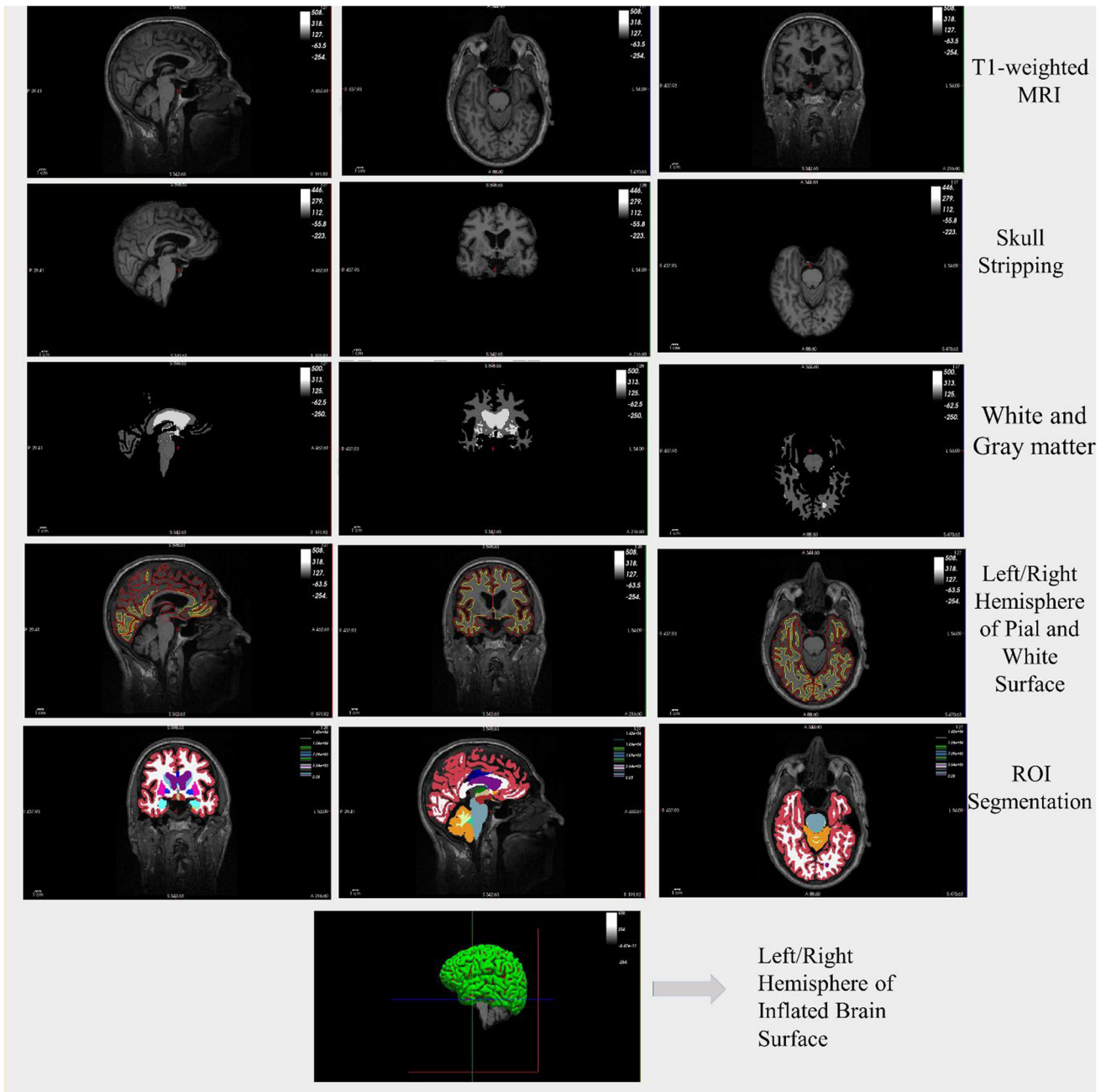


Fig. 3 ROI Segmentation of cortical and subcortical regions with VBM of White and Grey Matter in Brain

4.4 Feature selection

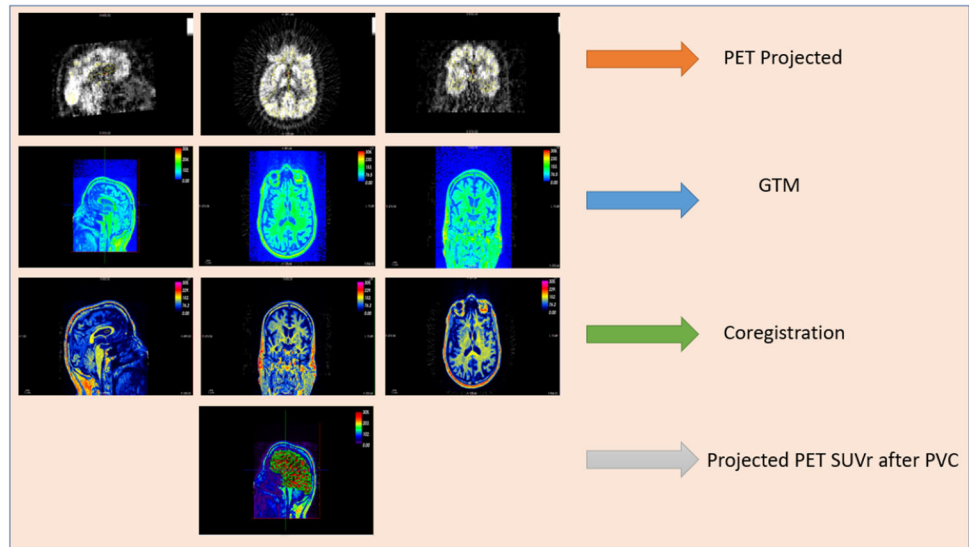
In this paper, 109 ROIs have been extracted from FDG-PET, PiB-PET, and MRI images to apply automatic feature extraction. Here, some features do not have any correlation with the output. These features take considerable computational time and space, making the performance degrades. The problems caused by extra features are referred to as the “curse of dimensionality”. Hence, overfitting occurs as a challenging task since the computation of features takes longer. By selecting the right parts, the dimensionality of

features can be reduced. As a result, the classification process is faster, which decreases the computational time in training and testing datasets, thereby facilitating classification accuracy. Firstly, the normalization of features is executed by Standard Scalar Function from 0.23.1 version of the Scikit-learn library [45]. After that, this dataset is transformed in such a way that data redundancy and dependency are reduced. Next, random tree embedding [46] is employed for high-dimensional data acquired from the Scikit-learn library (0.23.1) [45]. By using SelectKBest

Table 2 ROI Segmentation of Cortical and sub-cortical Regions of Brain

T1MRI biomarkers	ROI	Selected ROI Features	Label
Cortical Parcellation	Enorhinal (left + right)	White surface total area	WSTA
		mean thickness	MT
		surface area	ESA
		Thickness average	ETA
		thickness standard deviation	ETSD
		Mean curvature	EMC
		Folding index	EFI
	Parahippocampal (Left + Right)	Curvature index	ECI
		Surface area	PSA
		Thickness average	PTA
		thickness standard deviation	PTSD
		Mean curvature	PMC
		Folding index	PFI
		Curvature index	PCI
	Middle Temporal (Left + Right)	Surface area	MTSA
		Thickness average	MTTA
		Thickness standard deviation	MTTS
		Mean curvature	MTMC
		Folding index	MTFI
		Curvature index	MTCI
Inferior Temporal (Left + Right)		Surface area	ITSA
	Thickness average	ITTA	
	Thickness standard deviation	ITTS	
	Mean curvature	ITMC	
	Folding index	ITFI	
	Curvature index	ITCI	
	Subcortical Volume Features	RG/ LF Cerebellum White Matter	RGCWM/LFCWM
LF/ RG Thalamus Proper		LFTP/RGTP	
RG/LF Cerebellum Cortex		RGCC/LFCC	
LF/RG Putamen		LFP/RGP	
RG/LF Caudate		RGC/LFC	
LF/RG Pallidum		LFP/RGP	
LF /RG Amlygada		LFA/RGA	
LF/ RG Hippocampus		LFH/RGH	
RG/ LF Accumbens Area		RGAA/LFAA	
LF / RG Choroid Plexus		LFCP/RGCP	
LF /RG Ventral DC		LFVDC/RGVDC	
CSF	CSF		
T1WI MRI biomarkers	Selected ROI Features	Label	
<i>Global measure of brain</i>			
VBM (volume and intensity structure)	Brain segmentation volume	BSM	
	Volume of ventricles and choroid plexus	VVCP	
	Total cortical grey matter volume	TCGMV	
	Total cerebral white matter volume	TCWMV	

Fig. 4 Details of PET pipeline process of PVC



features from the Scikit learn library, we have selected the best features among them.

5 Classification methods

In this work, five different popular classifiers are used for evaluating performance based on single as well as combined features.

5.1 Adaptive HPT-RFE classifier

Random Forest is regarded as an ensemble machine learning algorithm where many decision trees are agglomerated for classification and regression tasks [47]. To overcome overfitting problems, different subsets of data are trained individual and then averaged value is taken.

In this work, Adaptive HPT-RFE classifier has been proposed and applied to the three binary classifications. The parameters adjusted in this method are `n_estimators` and `max_features`. The former parameter is defined as the number of trees. The time of computation is more for complicated trees. Beyond the critical trees, the results obtained are not significantly changing. The latter parameter is defined as the generation of random subsets when every node is being splatted. The default values of `max_features = 'Sqrt'` for the problems regarding classification. For achieving good results, `max_depth = None` along with `min_samples_split = 2`. Moreover, another parameter, `bootstrap = True`, is set as default, and `bootstrap = False` means extra trees are added. By setting `oob_score = True`, the generalization accuracy can be achieved by applying bootstrap sampling. For deciding the number of nodes in a particular branch of a decision tree, Gini Index plays important role for performance in

Random forests. To determine the value of Gini for a particular branch, a formula is framed which uses each class and probability that is most likely to occur.

$$Gini = 1 - \sum_{j=1}^N (p_j)^2 \tag{2}$$

here in this equation, N represents the number of classes in the dataset, p_j indicates the relative frequency of a particular class in the dataset. Importance of nodes is calculated for two child nodes which is given in equation.

$$N_k = w_{S_k} I_k + w_{L(k)} I_{L(k)} + w_{R(k)} I_{R(k)} \tag{3}$$

here N_k = node importance at k , w_{S_k} = weighted samples at node k , I_k = value of impurity at node k , $L(k)$ = left split at node k , $R(k)$ = right split at node k .

The calculation of each feature in random forest is given by:

$$FI = \frac{\sum_{k:\text{node } k \text{ splits the feature}} N_k}{\sum_{m \in \text{nodes}} N_m} \tag{4}$$

here FI = Feature Importance, N_k = Node Importance at k .

Then, features are normalised to value 0 and 1 by dividing all the features importance are

$$\text{normFI} = \frac{FI}{\sum_{k \in \text{all features}} FI_k} \tag{5}$$

The importance of all final features, at a level of Random Forest with Hyperparameter Tunning, is the sum total of average of decision trees. The resultant feature importance is given by the ratio of the sum of all feature importance to the total number of trees (T).

$$RFEC_k = \frac{\sum_{k \in \text{all features}} FI_{fk}}{T} \tag{6}$$

Pseudo code of Adaptive HPT-RFE classifier

Training phase

Input: Training Dataset $T_r(X, y)$ where X = Number of subjects, y = Classification Labels, number of estimators n_e , random state r_s , Class Number CN , Testing Dataset $T_{test}(X, y)$

Output: Classification Labels

```

for j in range (length of  $T_r$ ):
    def get_x_y ( $T_r(X, y)$ ):
        return [ $T_r(X, y)$ ]
    if data [ $CN$ ] == -1/0:
         $CN$ . append
    def model. Tree ( $X, y$ ):
         $X_{new}$ : SelectKBest(chi2) features from  $T_r(X, y)$ 
        clf: Create Random Forest Tree from  $n_e, r_s$ 
        return  $X_{new}, clf$ 
    end
end

```

Testing/Prediction Phase

```

for j in range (length of  $T_r$ ):
    def get_x_y ( $T_r(X, y)$ ):
        return [ $T_r(X, y)$ ]
    if data [ $CN$ ] == -1/0:
         $CN$ . append
    def model. Tree ( $X, y$ ):
         $X_{new}$ : SelectKBest(chi2) features from  $T_r(X, y)$ 
        clf: Create Random Forest Tree from  $n_e, r_s$ 
        return  $X_{new}, clf$ 
    end
end

```

5.2 SVM

For separating the two data groups, SVM is commonly used as a supervised machine learning algorithm for multivariate classification [48]. A hyperplane is required for classifying the data into various classes. Mathematically, it can be represented as

$$W \cdot X + b = 0 \quad (7)$$

where W represents as weight vectors, namely $W = \{P_1, P_2, P_3, \dots, P_N\}$; N indicates the number of features and b as the bias. As the bias term is influenced by the hyperplane, additional weight P_0 has been taken into consideration. Therefore, the above equation can be written as

$$P_0 + P_1X_1 + P_2X_2 + P_3X_3 + \dots + P_NX_N = 0 \quad (8)$$

If any point lies above the hyperplane, the equation is rewritten as

$$P_0 + P_1X_1 + P_2X_2 + P_3X_3 + \dots + P_NX_N > 0 \quad (9)$$

If any point lies below the hyperplane, the equation is rewritten as

$$P_0 + P_1X_1 + P_2X_2 + P_3X_3 + \dots + P_NX_N < 0 \quad (10)$$

For the above two equations, it can be understood that the “sides” of the SVM margin are written as

$$H1: P_0 + P_1X_1 + P_2X_2 + P_3X_3 + \dots + P_NX_N \geq 1 \text{ for } Y_i = +1 \quad (11)$$

$$H2: P_0 + P_1X_1 + P_2X_2 + P_3X_3 + \dots + P_NX_N \leq -1 \text{ for } Y_i = -1 \quad (12)$$

Combining the two inequalities of Eq. (11) and (12), we get

$$Y_i(P_0 + P_1X_1 + P_2X_2 + P_3X_3 + \dots + P_NX_N) \geq 1, \forall i \quad (13)$$

5.3 NBC

NBC [49] is a vital integrant in machine learning algorithm while considering calculation of the different set of probabilities with frequency counts. An assumption is made where all variables are mutually independent in classification problem [9]. The main idea behind NBC is on the basis of theorem of Bayes and total probabilities which is given by (11).

$$P(hp1|xi) = \frac{P(xi|hp1)P(hp1)}{(P(xi|hp1)P(hp1)) + (P(xi|hp2)P(hp2))} \tag{14}$$

where $P(hp1|xi)$ is posterior probability for hypothesis hp1. Prior probability for hypothesis hp1 and hp2 is given by $P(hp1)$ and $P(hp2)$, whereas $P(xi|hp1)$ and $P(xi|hp2)$ represent the likelihood of hp1 and hp2 hypothesis.

5.4 KNN

KNN is one of the nonparametric algorithms for machine learning. Here, instance data of training are stored by this classifier as Generalised Internal model is difficult to construct. At every point, classification values are computed by using majority vote. For every data class, assigned query point represents the most valued within k-NN [50]. A linear transformation matrix of size $n_features \times n_components$ maximizes the sum over the samples s with a probability P_s that are correctly classified as given in Eq. (15).

$$\arg \max_x \sum_{s=0}^{N-1} P_s \tag{15}$$

In the learned embedded space, probability P_s is given as

$$P_s = \sum_{k \in D_s} P_{sk} \tag{16}$$

where P_{sk} is defined as the softmax over Euclidean Distance and D_s are the set of points that belong to same class for each sample.

5.5 ANN

ANN is a computational scheme which as a representation of biological neural networks existed in human brains which is expressed through connected nodes [51]. In the architecture of ANN, nonlinear activation function is used in a feedforward structure. Biases are added in each layer for finding outputs in the layer (Z_k) using mathematical expressions.

$$N_j = \sum_{i=1}^d x_i w_{ij} + B \tag{17}$$

$$N_k = \sum_{j=1}^{nH} y_j w_{kj} + B \tag{18}$$

$$Z_k = f \left(\sum_{j=1}^{nH} y_j w_{kj} f \left(\sum_{i=1}^d x_i w_{ij} + B \right) + B \right) \tag{19}$$

Description of Adaptive HPT-RFE Algorithm
<p>Training Phase:</p> <p>Input: Tr: Training set with f features and target variable N: number of classes in target variable Cl: Number of Classifiers</p> <p>Procedure:</p> <p>For b=1 to Cl // Cl=5</p> <ol style="list-style-type: none"> 1. Generate bootstrap Sample S* from the training set Tr 2. Append random forest tree (RFT) from S*, by repeating all the steps for terminal node. <p>For a particular node (pn),</p> <ol style="list-style-type: none"> i. Select (K pn/5) best features ii. Pick the Kth feature from chi2 test iii. Split the nodes for Kth feature <p>Repeat (i) to (iii) till the minimum nodes n_{min} is reached</p> <ol style="list-style-type: none"> 3. Construct the trained classifiers Cl // Cl=5 <p>Testing Phase:</p> <p>Aggregate all Cl trained classifiers using majority vote for predicting the class label C_L.</p> <p>$C_L = \arg \max_b \sum_{b=1}^{Cl=5} I(C_L(x) = k)$, for $k=1, \dots, M$ testing datapoints</p>

Fig. 5 Flow chart of adaptive HPT-RFE algorithm for training and testing data

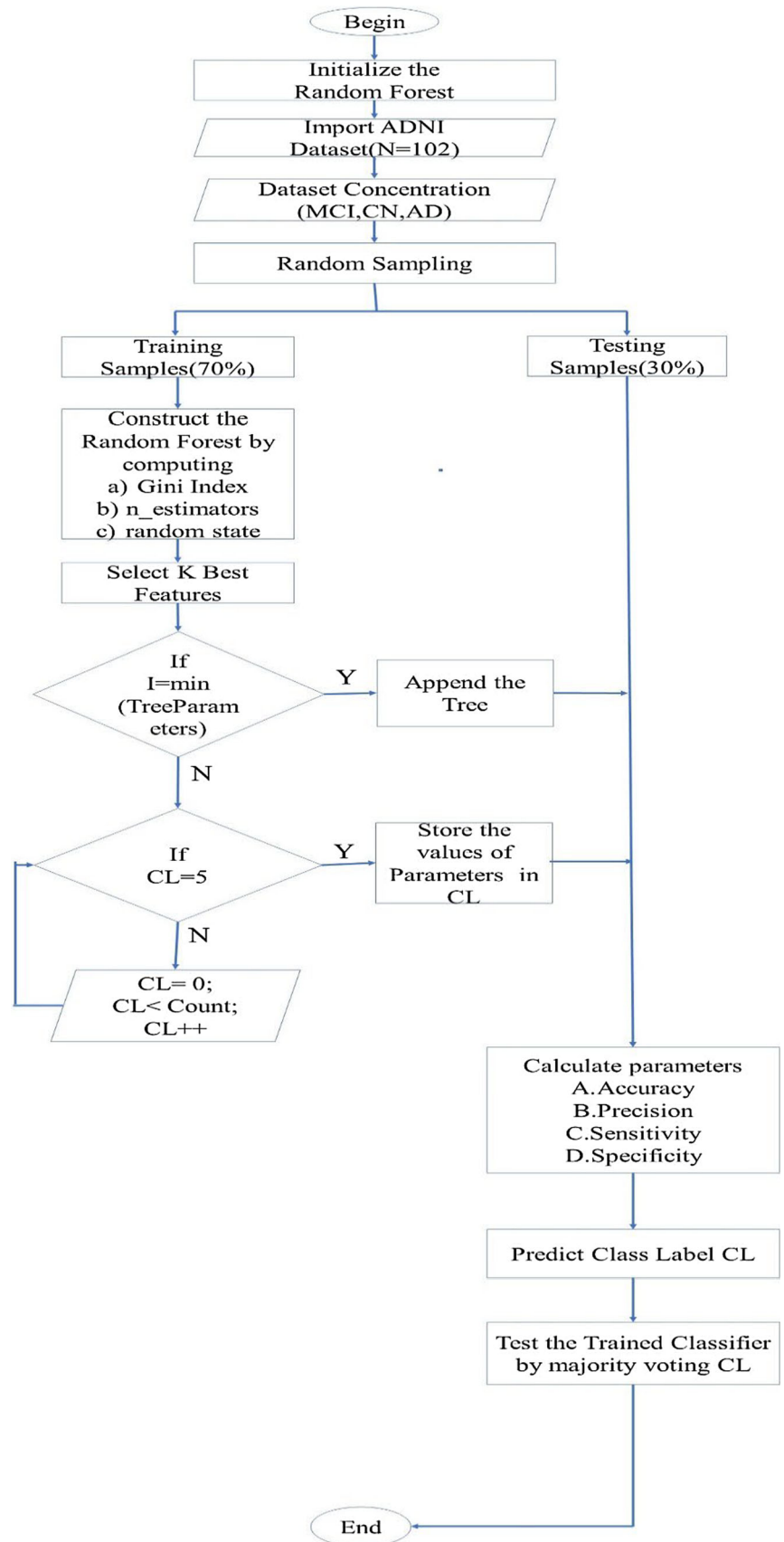


Table 3 Results on three binary classifications

Classifier	ACC	SENS	SPEC	PREC	F1SC
<i>AD versus NC</i>					
HPT-RFE	100	100	100	100	100
K Nearest Neighbour	77	80	75	66	72
Naïve Bayes	62	100	37.5	50	66.67
Artificial neural Network	85	80	75	80	80
SVM	77	80	75	66.67	72.72
<i>MCI versus AD</i>					
HPT-RFE	95	80	100	100	88.88
K Nearest Neighbour	73	20	88	33	25
Naïve Bayes	77	Versus	100	Versus	Versus
Artificial neural Network	91	60	100	100	75
SVM	77	Versus	100	Versus	Versus
Classifier	ACC	SENS	SPEC	PREC	F1SC
HPT-RFE	91	60	100	100	75
K Nearest Neighbour	77	80	75	66	72
Naïve Bayes	77	Versus	100	Versus	Versus
Artificial neural Network	59	40	64	25	30
SVM	77	Versus	100	Versus	Versus
<i>MCI versus NC</i>					
HPT-RFE	91	60	100	100	75
K Nearest Neighbour	77	80	75	66	72
Naïve Bayes	77	–	100	–	–
Artificial neural Network	59	40	64	25	30
SVM	77	–	100	–	–

6 Results and discussion

6.1 Experimental evaluation

For addressing the K-best features, i.e., one versus one binary classification tasks such as AD versus NC, MCI versus NC, AD versus MCI, five classifiers have been applied on sagittal, axial and coronal orientations of T1WI MRI images. Here, 102 subjects are acquired from the ADNI database which has been considered in our study. The samples are randomized so that 70% of the samples are trained, and 30% are used for testing. Random forest tree is generated by calculating Gini Index and tuning hyperparameters such as Random state and number of estimators trained by five Classifiers. Hence, Accuracy, Precision, Sensitivity, and Specificity are calculated from the Confusion Matrix of testing samples. By using the majority voting of the classifier, classification labels are identified. The detailed procedure of experimentation is given in Fig. 5.

6.2 Performance evaluation metrics

For evaluating performance metrics, diagonal elements of the Confusion matrix represent rightly predicted by the classifier. These elements are further divided into True Positive (TP) and True Negative (TN) correctly labelled. False Negative (FN) and False Positive (FP) are non-diagonal elements for incorrectly labelled classes. Accuracy (ACC), Sensitivity (SEN), Specificity (SPEC), F1 Score (F1SC), and Precision (PREC) are defined as follows [52]:

$$\text{ACC} = \frac{\text{TP} + \text{TN}}{(\text{TP} + \text{TN} + \text{FP} + \text{FN})} \quad (20)$$

$$\text{PREC} = \frac{\text{TP}}{\text{TP} + \text{FN}} \quad (21)$$

$$\text{SPEC} = \frac{\text{TN}}{\text{TN} + \text{FA}} \quad (22)$$

$$\text{SENS} = \frac{\text{TP}}{\text{TP} + \text{FP}} \quad (23)$$

$$\text{F1SC} = \frac{2 \text{TP}}{2 \text{TP} + \text{FP} + \text{FN}} \quad (24)$$

Features are extracted from different modalities and converted into a vector consisting of a single feature where classifiers are trained on a particular feature vector. Functions are called for importing libraries from Scikit Learn 0.23.1 in tuning the hyperparameters executed on Python IDE 3.6 environment. Hence, each optimized hyperparameter is trained in five different classifiers for the training dataset and then evaluating the model's performance using the test dataset. The given experiments are run on the system having the configuration of OS Windows 10, Intel® Core™ i7-9750U CPU @ 2.60 GHz processor, six-core, 12 Logical Processors, and 16 GB RAM with Ubuntu 20.04.2. Summarisation of classification report of three binary classification is shown in Table 3.

For evaluating various diagnostic tests in biomedical research for testing the performance in classification problems and different prediction models, Accuracy of ROC Curve (ROC-AUC) is used as a fundamental graph. Therefore, the ROC-AUC plot has True positive rate (TPR) and False Positive Rate (FPR) parameters which are performance measure in positive and negative part of the dataset. ROC curves have been drawn for each classifier model for three binary classifications such as AD versus NC, AD versus MCI and MCI versus NC which is given in Fig. 6.

6.3 Comparison with other state-of-the-art techniques

Detecting AD right its onset has been a significant problem in the process of AD diagnosis. Most of the past work has achieved sufficient accuracy in classifying whether a subject has AD or normal [51]. However, the binary classification of AD versus MCI and MCI versus NC is still an open problem for the community of researchers. The result obtained from the proposed work for three binary classifications of AD versus MCI, MCI versus NC, and NC versus AD is reported in Tables 4, 5 and 6. The modalities of the proposed work given in Tables 4, 5 and 6 only mention the image-based biomarkers however the work also includes the quantitative values of cognitive assessments. It is instinctive that differentiating between NC and AD should be more accessible, which is also evident in our results as the binary classification of AD versus NC has been achieved 100% accuracy. The accuracy of the other two binary classifications: AD versus MCI and NC versus MCI, has achieved 95% and 91%, respectively. Compared to the classification of AD versus NC, this reduction inaccuracy is because the features obtained after segmentation of cortical and subcortical regions and the SUVR are not as distinct for MCI and AD subjects.

The results obtained also justify the use of the quadruple biomarkers. The accuracy, specificity and sensitivity values generated by the proposed work have been compared with the state-of-the-art techniques and given in Tables 4, 5 and 6. Table 4 shows a comparison with previous researches which have used a single biomarker, Table 5 shows a comparison of previous works using a combination of two biomarkers and Table 6 shows a comparison with techniques using triple biomarkers. Most of the works mentioned in Tables 4, 5 and 6 have worked on ADNI or a dataset that is similar to the ADNI dataset. It can be seen that the accuracies reported by previous works which have used either single, double, and triple biomarkers are less compared to the proposed work. Therefore, it can infer that the quadruple biomarkers are more efficient in early diagnosing of AD. Another observation from the obtained result is that the system's sensitivity is lesser than the specificity for all three binary classifications. This would mean that the system can prevent a more significant number of misdiagnoses which is also seen in most previous works. The author would analyse the effect of considering multiple biomarkers on specificity and improve it in future work.

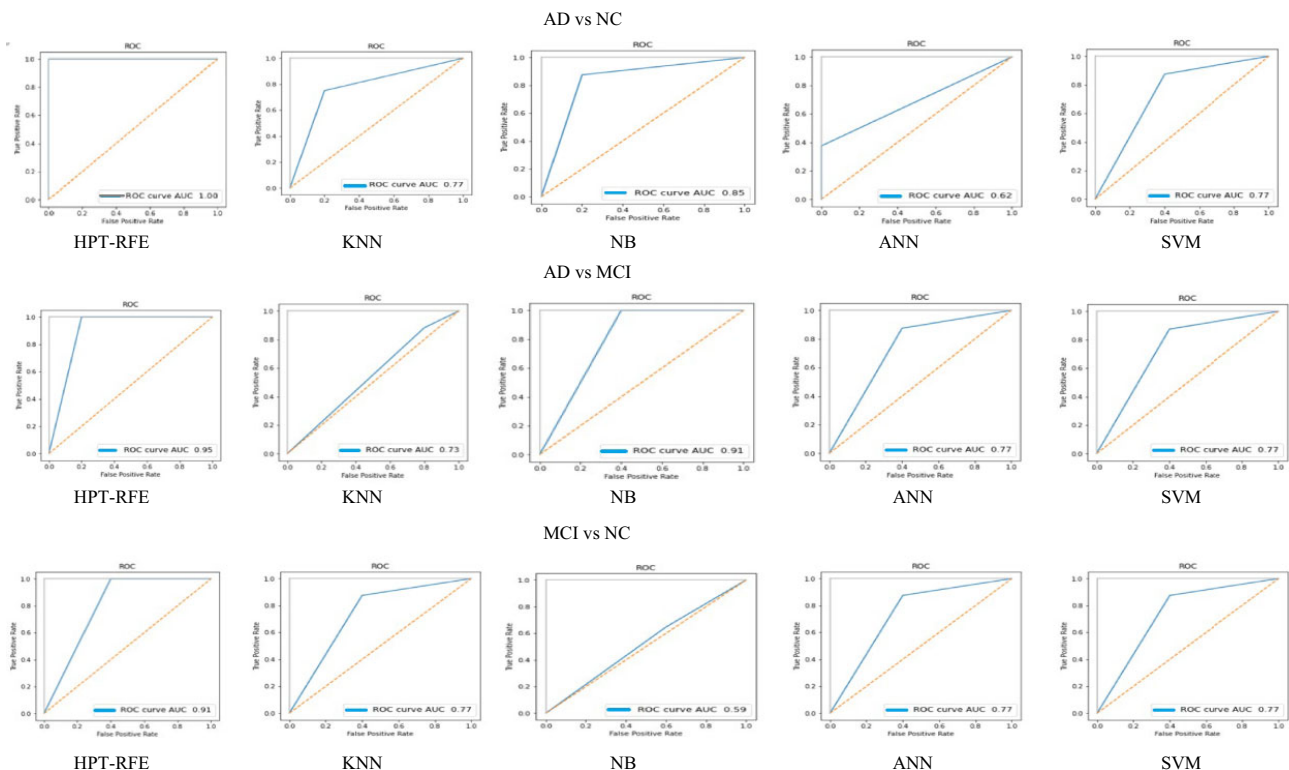


Fig. 6 ROC Curves for adaptive HPT-RFE, KNN, NB, ANN and SVM classifiers in each binary classification

Table 4 Comparison of results obtained using the proposed model with other state-of-the-art methods using single biomarkers

Categories	Model	Classifier	Modalities	Accuracy	Specificity	Sensitivity
AD versus NC	Beheshti and Demirel [53]	SVM	MRI	92.48	93.89	91.07
	Jha et al. [54]	ELM	MRI	90.26	91.07	90.26
	Gupta et al. [55]	SVM	MRI	96.42	100	93.8
	Mehmood et al. [56]	VGG Architecture	MRI	98.73	–	–
	Furst et al. [57]	<i>T</i> -test	FDG-PET	–	85	75
	Veen et al. [58]	LGMLVQ	FDG-PET	–	91.45	91.47
	Gupta et al. [59]	Kernel-A SVM	FDG-PET	92.5	90	89.74
	Martino et al. [58]	GMLVQ and SVM	FDG-PET	–	84	80
	Furst et al. [57]	<i>T</i> test	PiB-PET	–	82	90
	Orit H et al. [60]	SVM	PiB-PET	–	86	96
	Yi et al. [61]	GLM univariate analysis	PiB-PET	88	71	94
	Giacomucci et al. [62]	Kolmogorov smirnov test	PiB-PET	86.21	78.95	89.74
		Proposed model	HPT-RFE	MRI + FDG-PET + PiB-PET + Cognitive assessments	100	100
NC versus MCI	Gupta et al. [55]	KNN	MRI	81.48	92.3	71.42
	Salvatore et al. [63]	Linear SVM	MRI	72	69	75
	Mehmood et al. [56]	VGG Architecture	MRI	80	–	–
	Liu et al. [64]	Cox and Decision Tree	MRI	68.8	74.07	64.29
	Liu et al. [64]	Cox and Decision Tree	FDG-PET	68.8	82.41	57.14
	Zhu et al. [65]	Support Vector Regression	FDG-PET	71.2	93	47.14
	Lu et al. [66]	Deep Neural Network	FDG-PET	81.53	82.47	78.2
	Gupta et al. [59]	SVM	FDG-PET	91.07	100	88.46
	Wei-Wei Li et al. [67]	ANOVA test	PiB-PET	77	82	64
	Vandenberghé et al. [68]	Probabilistic Analysis	PiB-PET	–	100	92
	Lowe et al. [69]	Fischer Test	PiB-PET	90	–	–
	Daoqiang et al. [70]	SVM	PiB-PET	76.4	66	81.8
		Proposed model	HPT-RFE	MRI + FDG-PET + PiB-PET + Cognitive assessments	91	100
AD versus MCI	Rallabandi et al. [71]	Nonlinear SVM	MRI	75	77	75
	Gupta et al. [55]	KNN	MRI	65.21	75	60
	Mehmood et al. [56]	VGG Architecture	MRI	83.72	–	–
	Kitajima et al. [72]	Mc Nemar Test	MRI	73.1	80	68.8
	Martinez et al. [73]	ANOVA Test	FDG-PET	–	69	64
	Ding et al. [74]	Deep Neural Network	FDG-PET	73	73	59
	Gupta et al. [59]	Kernel-Based Multiclass SVM	FDG-PET	84.03	88.24	66.67
	Zhang et al. [75]	Moses Shapiro Littenverg	FDG-PET	–	74	78.7
	Zhang et al. [75]	Moses Shapiro Littenverg	PiB-PET	–	56.2	93.5
	Yan Ma [76]	Spearman Test	PiB-PET	–	41.1	83.3
	Li et al. [61]	Automated ROI	PiB-PET	67	69	65
	Kitajima et al. [72]	Mc Nemar Test	PiB-PET	66.7	83.3	73.3
		Proposed model	HPT-RFE	MRI + FDG-PET + PiB-PET + Cognitive assessments	95	100

Table 5 Comparison of results obtained using the proposed model with other state-of-the-art methods using two biomarkers

Categories	Model	Classifier	Modalities	Accuracy	Specificity	Sensitivity
AD vs NC	Peng et al. [77]	Descent algorithm	MRI + FDG-PET	96.1	94.9	97.3
	Suk et al. [78]	Stacked autoencoder	MRI + FDG-PET	95.09	98	92
	Zheng et al. [79]	Particle swarm optimisation (PSO)	MRI + FDG-PET	88.52	92.2	84.6
	Kim et al. [80]	Multimodal sparse hierarchical extreme learning machine (MSH-ELM)	MRI + FDG-PET	97.2	94.12	98.08
	Chételat et al. [81]	Diagnostic algorithm	PiB-PET + FDG-PET	–	100	96
	Orit H et al. [60]	SVM	PiB-PET + FDG-PET	–	98	97
	Suppiah et al. [82]	Pearson chi square correlation test	PiB-PET + FDG-PET	–	77.4	62.5
	Proposed model	HPT-RFE	MRI + FDG-PET + PiB-PET + Cognitive assessments	100	100	100
NC vs MCI	Zhang et al. [83]	Linear regression	MRI + FDG-PET	76.8	68	79
	Suk et al. [84]	Deep Boltzmann Machine	MRI + FDG-PET	74.66	95.23	48.04
	Lui et al. [64]	cox model	MRI + FDG-PET	80.8	70.37	76.19
	Wang et al. [85]	Random forest	MRI + FDG-PET	73.64	–	–
	Devanand et al. [86]	ANOVA test	PiB-PET + FDG-PET	–	71	81
	Yang et al. [87]	Deep learning	PiB-PET + FDG-PET	–	77.63	91.02
	Ortiz et al. [88]	Deep belief network	PiB-PET + FDG-PET	84	89	79
	Vandenbergh et al. [89]	SVM	PiB-PET + FDG-PET	100	92	85.2
Proposed model	HPT-RFE	MRI + FDG-PET + PiB-PET + Cognitive assessments	91	100	60	
AD vs MCI	Sivapriya et al. [90]	Random forest	MRI + FDG-PET	96.3	–	–
	Peng et al. [77]	Coordinate descent algorithm	MRI + FDG-PET	76.9	82.7	65.9
	Cheng et al. [91]	Domain transfer support vector machine	MRI + FDG-PET	80.1	73.3	85.3
	Suk et al. [78]	Stacked autoencoder	MRI + FDG-PET	74.15	92.67	50.5
	Mosconi et al. [92]	Diagnostic test	PiB-PET + FDG-PET	80	50	50
	Li wei et al. [67]	ANOVA TEST	PiB-PET + FDG-PET	77	64	82
	Rabinovici et al. [93]	Student <i>t</i> test	PiB-PET + FDG-PET	–	83	89
	Proposed model	HPT-RFE	MRI + FDG-PET + PiB-PET + Cognitive assessments	95	100	80

7 Conclusion and future work

In this study, Adaptive HPT-RFE Classifier has been proposed for one versus one three binary classifications using single modality features (MRI, FDG-PET, PiB-PET) or

multi-modality features (MRI and FDG-PET, FDG-PET and PiB-PET, MRI, FDG-PET and PiB-PET). Here, FreeSurfer Software is used in HPC to extract features of MRI, FDG-PET, PiB-PET Images from 102 subjects. Best classification accuracy, sensitivity, and specificity results are

Table 6 Comparison of results obtained using the proposed model with other state-of-the-art methods using three biomarkers

Categories	Model	Classifier	Modalities	Accuracy	Specificity	Sensitivity
AD versus NC	Ortiz et al. [88]	Deep belief network	MRI + FDG-PET + PiB-PET	92	86	96
	Gupta et al. [59]	Kernel-based multiclass SVM	MRI + FDG-PET + PiB-PET	98.33	96.47	100
	Tong et al. [94]	SVM	MRI + FDG-PET + PiB-PET	91.8	94.7	88.9
	Zhang et al. [70]	Linear SVM	MRI + FDG-PET + PiB-PET	93.2	93.3	93
	Proposed Model	HPT-RFE	MRI + FDG-PET + PiB-PET + cognitive assessments	100	100	100
NC versus MCI	Young et al. [95]	Bayesian	MRI + FDG-PET + PiB-PET	79.5	65.6	78.7
	Cheng et al. [91]	Domain transfer support vector machine	MRI + FDG-PET + PiB-PET	84.8	72.7	84.5
	Gupta et al. [59]	Kernel-based multiclass SVM	MRI + FDG-PET + PiB-PET	98.33	96.47	100
	Moradi et al. [96]	Semi supervised learning method	MRI + FDG-PET + PiB-PET	90.2	73.64	86.65
	Proposed Model	HPT-RFE	MRI + FDG-PET + PiB-PET + cognitive assessments	91	100	60
AD versus MCI	Teng et al. [97]	RBF-SVM	MRI + FDG-PET + PiB-PET	88.61	93.48	81.82
	Ortiz et al. [88]	Deep belief network	MRI + FDG-PET + PiB-PET	84	81	87
	Tong et al. [94]	SVM	MRI + FDG-PET + PiB-PET	60.26	–	–
	Gupta et al. [59]	Kernel-based multiclass SVM	MRI + FDG-PET + PiB-PET	94.64	92.86	91.67
	Proposed model	HPT-RFE	MRI + FDG-PET + PiB-PET + cognitive assessments	95	100	80

produced while comparing four different classifiers for each binary classification problem. Also, this technique performs best for comparison with other state-of-the-art methods. Therefore, these results indicate that it may be beneficial as a potential tool for diagnosing the different Alzheimer's disease classes.

Meanwhile, there are other learning techniques such as deep learning algorithms such as hybrid architectures of Convolutional Neural Networks (CNNs) [70], Long Short-Term Memory (LSTM), Deep Autoencoders (DAE), and more variants of Artificial Neural Networks (ANN) could be used in future works for getting much-improved classification accuracy for all various classes of AD. Moreover, an amalgamation of feature selection techniques and deep learning models would be applied on single modality and multi modalities, which can be addressed as a future problem mainly focussing on the interpretability of clinical diagnosis. Also, researchers are primarily concentrating on

the methods based on feature selection but not in the classification of AD from NC.

In the future, the colossal size of the dataset can be applied for classification purposes. In addition to that, other machine learning tools can be used. Hence, these models can also be learned to diagnose other diseases such as Parkinson's disease, Brain Cancer, Eplisey, asthma, and blood cancer. Based on this idea, different ensemble models can be generated for increasing the performance in the classification of other datasets, such as text mining, text classification, which is written in various languages and formats.

Declarations

Conflict of interest All the authors declare that they have no conflict of interest related to this review. This article does not contain any

studies with human or animal subjects performed by the any of the authors.

References

- Thies W, Bleiler L (2013) 2013 Alzheimer's disease facts and figures. *Alzheimers Dement* 9(2):208–245
- 2016 Alzheimer's disease facts and figures. (2016). *Alzheimer's Dementia*, 12(4), 459–509
- Alzheimer's Disease. (2010). *New England J Med* 362(19), 1844–1845
- Jack C, Knopman D, Jagust W, Shaw L, Aisen P, Weiner M et al (2010) Hypothetical model of dynamic biomarkers of the Alzheimer's pathological cascade. *Lancet Neurol* 9(1):119–128
- Li X, Li T, Andreassen N, Wiberg M, Westman E, Wahlund L (2013) The association between biomarkers in cerebrospinal fluid and structural changes in the brain in patients with Alzheimer's Disease. *J Intern Med* 275(4):418–427
- Perez-Nievas B, Stein T, Tai H, Dols-Icardo O, Scotton T, Barroeta-Espar I et al (2013) Dissecting phenotypic traits linked to human resilience to Alzheimer's pathology. *Brain* 136(8):2510–2526
- Birch A, Katsouri L, Sastre M (2014) Modulation of inflammation in transgenic models of Alzheimer's disease. *J Neuroinflamm*. <https://doi.org/10.1186/1742-2094-11-25>
- Karch C, Goate A (2015) Alzheimer's disease risk genes and mechanisms of disease pathogenesis. *Biol Psychiat* 77(1):43–51
- Brayne C (2014) A population perspective on the IWG-2 research diagnostic criteria for Alzheimer's disease. *Lancet Neurol* 13(6):532–534
- Park S, Kim J, Kim H, Kim T, Kim Y, Lee D et al (2013) Preliminary study for a multicenter study of Alzheimer's disease cerebrospinal fluid biomarkers. *Dementia Neurocognit Disorder* 12(1):1
- Bandelow S, Clifford A, Wardt V, Hogervorst E, Madden M, Lindsay J, Gale A (2011) P1–139: Accurate non-invasive diagnoses of Alzheimer's Disease using eye scanning. *Alzheimer's Dementia*. <https://doi.org/10.1016/j.jalz.2011.05.419>
- Barthel H, Schroeter M, Hoffmann K, Sabri O (2015) PET/MR in dementia and other neurodegenerative diseases. *Semin Nucl Med* 45(3):224–233
- Kumari R, Pushkar S (2020) Analysis of biomedical image for Alzheimers disease detection. In: *Examining Fractal Image Processing and Analysis Advances in Computational Intelligence and Robotics*, 224–251
- Jadvar H, Colletti P (2014) Competitive advantage of PET/MRI. *Eur J Radiol* 83(1):84–94
- Klunk WE, Engler H, Nordberg A, Wang Y, Blomqvist G, Holt DP, Långström B (2004) Imaging brain amyloid in Alzheimers disease with Pittsburgh compound-B. *Ann Neurol* 55(3):306–319
- Thal DR, Rüb U, Orantes M, Braak H (2002) Phases of A β -deposition in the human brain and its relevance for the development of AD. *Neurology* 58(12):1791–1800
- Braak H, Braak E (1990) Alzheimer's disease. *J Neuropathol Exp Neurol* 49(3):215–224
- Edison P, Archer HA, Hinz R, Hammers A, Pavese N, Tai YF, Brooks DJ (2006) Amyloid, hypometabolism, and cognition in Alzheimer disease: An [11C] PIB and [18F] FDG PET study. *Neurology* 68(7):501–508
- Bråne G, Gottfries CG (1986) The GBS scale: a new rating scale for dementia syndromes. *Nord Psykiatr Tidsskr* 40(2):125–134
- Morris JC, Ernesto C, Schafer K, Coats M, Leon S, Sano M, Woodbury P (1997) Clinical dementia rating training and reliability in multicenter studies. *Neurology* 48(6):1508–1510
- Mckhann GM, Knopman DS, Chertkow H, Hyman BT, Jack CR, Kawas CH, Phelps CH (2011) The diagnosis of dementia due to Alzheimers disease: recommendations from the National Institute on Aging-Alzheimers Association workgroups on diagnostic guidelines for Alzheimers disease. *Alzheimers Dementia* 7(3):263–269
- Podhorna J, Krahnke T, Shear M, Harrison JE (2016) Alzheimer's disease assessment scale-cognitive subscale variants in mild cognitive impairment and mild Alzheimer's Disease: change over time and the effect of enrichment strategies. *Alzheimers Res Therapy*. <https://doi.org/10.1186/s13195-016-0170-5>
- Stern Y (2012) Cognitive reserve in ageing and Alzheimers disease. *Lancet Neurol* 11(11):1006–1012
- Morris JC, Selkoe DJ (2011) Recommendations for the incorporation of biomarkers into Alzheimer clinical trials: an overview. *Neurobiol Aging* 32:S1
- Grimmer T, Riemenschneider M, Förstl H, Henriksen G, Klunk WE, Mathis CA, Drzezga A (2009) Beta amyloid in Alzheimers disease: increased deposition in brain is reflected in reduced concentration in cerebrospinal fluid. *Biol Psychiat* 65(11):927–934
- Drzezga A, Barthel H, Minoshima S, Sabri O (2014) Potential clinical applications of PET/MR imaging in neurodegenerative diseases. *J Nuclear Med* 55(Supplement 2):47S-55S. <https://doi.org/10.2967/jnumed.113.129254>
- Zhang XY, Yang ZL, Lu GM, Yang GF, Zhang LJ (2017) PET/MR imaging: new frontier in Alzheimers disease and other dementias. *Front Mol Neurosci*. <https://doi.org/10.3389/fnmol.2017.00343>
- <http://adni.loni.usc.edu/>
- <http://www.adni-info.org>
- <http://adni.loni.usc.edu/methods/mri-tool/mri-analysis>
- <http://adni.loni.usc.edu/pet-analysis-method/pet-analysis>
- <http://adni.loni.usc.edu/pibpet-analysis-method/pibpet-analysis>
- Fischl B (2012) FreeSurfer. *Neuroimage* 62(2):774–781
- https://www.bitmesra.ac.in/Visit_Department_Page?cid=1&deptid=70&pid=112
- Ashburner J, Friston KJ (2001) Why voxel-based morphometry should be used. *Neuroimage* 14(6):1238–1243
- Whitwell JL (2009) Voxel-based morphometry: an automated technique for assessing structural changes in the brain. *J Neurosci* 29(31):9661–9664
- Schmitter D, Roche A, Maréchal B, Ribes D, Abdulkadir A, Bach-Cuadra M, Krueger G (2015) An evaluation of volume-based morphometry for prediction of mild cognitive impairment and Alzheimers disease. *NeuroImage Clin* 7:7–17
- <http://surfer.nmr.mgh.harvard.edu>
- Fischl B, Salat DH, Kouwe AJ, Makris N, Ségonne F, Quinn BT, Dale AM (2004) Sequence-independent segmentation of magnetic resonance images. *NeuroImage* 23:S69
- Lancaster J, Kochunov P, Nickerson D, Fox P (2000) Stand-alone Java-based version of the Talairach daemon database system. *NeuroImage* 11(5):S923
- Minoshima S, Frey KA, Foster NL, Kuhl DE (1995) Preserved pontine glucose metabolism in Alzheimer disease. *J Comput Assist Tomogr* 19(4):541–547
- Erlandsson K, Irène Buvat P, Pretorius H, Thomas BA, Hutton BF (2012) A review of partial volume correction techniques for emission tomography and their applications in neurology, cardiology and oncology. *Phys Med Biol* 57(21):R119–R159. <https://doi.org/10.1088/0031-9155/57/21/R119>
- Thomas BA, Cuplov V, Bousse A, Mendes A, Thielemans K, Hutton BF, Erlandsson K (2016) PETPVC: a toolbox for performing partial volume correction techniques in positron emission tomography. *Phys Med Biol* 61(22):7975–7993

44. Fischl B, Sereno MI, Tootell RB, Dale AM (1999) High-resolution intersubject averaging and a coordinate system for the cortical surface. *Hum Brain Mapp* 8(4):272–284
45. Pedregosa F, Varoquaux G, Gramfort A, Michel V, Thirion B, Grisel O, Blondel M et al (2011) Scikit-learn: machine learning in python. *J Mach Learn Res* 12:2825–2830
46. Geurts P, Ernst D, Wehenkel L (2006) Extremely randomized trees. *Mach Learn* 63(1):3–42
47. Lebedev A, Westman E, Westen GV, Kramberger M, Lundervold A, Aarsland D, Simmons A (2014) Random forest ensembles for detection and prediction of Alzheimers disease with a good between-cohort robustness. *NeuroImage Clin* 6:115–125
48. Cuingnet R, Gerardin E, Tessieras J, Auzias G, Lehéricy S, Habert M, Colliot O (2011) Automatic classification of patients with Alzheimers disease from structural MRI: a comparison of ten methods using the ADNI database. *Neuroimage* 56(2):766–781
49. Seref B, Bostanci E (2019) Performance comparison of naïve bayes and complement naïve bayes algorithms. In: 2019 6th international conference on electrical and electronics engineering (ICEEE)
50. Dinu A.J (2019) Early detection of alzheimers disease using predictive K-NN instance based approach and T-Test method. *Int J Adv Trends Comput Sci Eng* 8:29–37
51. Bersimis FG, Varlamis I (2019) Use of health-related indices and classification methods in medical data. *Classif Tech Med Image Anal Comput Aided Diagnos* 2019:31–66
52. Gupta Y, Lee KH, Choi KY, Lee JJ, Kim BC, Kwon GR (2019) Early diagnosis of Alzheimer’s disease using combined features from Voxel-based morphometry and cortical, subcortical, and hippocampus regions of MRI T1 brain images. *Plos One* 14(10):e0222446
53. Beheshti I, Demirel H (2016) Feature-ranking-based Alzheimer’s disease classification from structural MRI. *Magn Reson Imaging* 34(3):252–263
54. Jha D, Alam S, Pyun J, Lee KH, Kwon G (2018) Alzheimers disease detection using extreme learning machine, complex dual tree wavelet principal coefficients and linear discriminant analysis. *J Med Imaging Health Inf* 8(5):881–890
55. Gupta Y, Lee KH, Choi KY, Lee JJ, Kim BC, Kwon GR (2019) Early diagnosis of Alzheimer’s Disease using combined features from voxel-based morphometry and cortical, subcortical, and hippocampus regions of MRI T1 brain images. *Plos One* 14(10):e0222446
56. Mehmood A, Yang S, Feng Z, Wang M, Ahmad AS, Khan R, Yaqub M (2021) A transfer learning approach for early diagnosis of alzheimer’s disease on MRI images. *Neuroscience* 460:43–52
57. Furst AJ, Agarwal N, Mormino EC (2011) Amyloid vs FDG-PET in the differential diagnosis of AD and FTLD. *Neurology* 77(23):2034–2042
58. Martino-IST IT, Navarra ES (2018) Machine learning based analysis of FDG-PET image data for the diagnosis of neurodegenerative diseases. *Appl Intell Syst Proc Int APPIS Conf* 310:280
59. Gupta Y, Lama RK, Kwon G (2019) Prediction and classification of Alzheimer’s disease based on combined features from apolipoprotein-E genotype, cerebrospinal fluid, MR, and FDG-PET imaging biomarkers. *Front Comput Neurosci*. <https://doi.org/10.3389/fncom.2019.00072/full>
60. Lesman-Segev OH, La Joie R, Iaccarino L, Lobach I, Rosen HJ, Seo SW, Janabi M et al (2021) Diagnostic accuracy of amyloid versus 18f-fluorodeoxyglucose positron emission tomography in autopsy-confirmed dementia. *Ann Neurol* 89(2):389–401
61. Li Y, Rinne JO, Mosconi L, Pirraglia E, Rusinek H, Desanti S, Leon MJ (2008) Regional analysis of FDG and PIB-PET images in normal aging, mild cognitive impairment, and Alzheimer’s disease. *Eur J Nucl Med Mol Imaging* 35(12):2169–2181
62. Giacomucci G, Mazzeo S, Bagnoli S, Casini M, Padiglioni S, Polito C, Bessi V (2021) Matching clinical diagnosis and amyloid biomarkers in Alzheimer’s disease and frontotemporal dementia. *J Personal Med* 11(1):47
63. Salvatore C, Cerasa A, Castiglioni I (2018) MRI characterizes the progressive course of ad and predicts conversion to Alzheimer’s dementia 24 months before probable diagnosis. *Front Aging Neurosci*. <https://doi.org/10.3389/fnagi.2018.00135>
64. Liu K, Chen K, Yao L, Guo X (2017) Prediction of mild cognitive impairment conversion using a combination of independent component analysis and the cox model. *Front Hum Neurosci*. <https://doi.org/10.3389/fnhum.2017.00033>
65. Zhu X, Suk H, Wang L, Lee S, Shen D (2017) A novel relational regularization feature selection method for joint regression and classification in AD diagnosis. *Med Image Anal* 38:205–214
66. Lu D, Popuri K, Ding GW, Balachandar R, Beg MF (2018) Multimodal and multiscale deep neural networks for the early diagnosis of Alzheimer’s Disease using structural MR and FDG-PET images. *Sci Rep*. <https://doi.org/10.1038/s41598-018-22871-z>
67. Li W, Shen Y, Tian D, Bu X, Zeng F, Liu Y, Wang Y (2019) Brain Amyloid- β deposition and blood biomarkers in patients with clinically diagnosed Alzheimer’s disease. *J Alzheimers Dis* 69(1):169–178
68. Vandenberghe R, Adamczuk K, Dupont P, Laere KV, Chételat G (2013) Amyloid PET in clinical practice: its place in the multi-dimensional space of Alzheimers disease. *NeuroImage Clin* 2:497–511
69. Lowe VJ, Kemp BJ, Jack CR, Senjem M, Weigand S, Shiung M, Petersen RC (2009) Comparison of 18F-FDG and PiB PET in Cognitive Impairment. *J Nucl Med* 50(6):878–886
70. Zhang D, Wang Y, Zhou L, Yuan H, Shen D, Initiative ADN (2011) Multimodal classification of Alzheimer’s Disease and mild cognitive impairment. *Neuroimage* 55(3):856–867
71. Rallabandi VS, Tulpule K, Gattu M (2020) Automatic classification of cognitively normal, mild cognitive impairment and Alzheimers disease using structural MRI analysis. *Inf Med Unlocked* 18:100305
72. Kitajima K, Abe K, Takeda M, Yoshikawa H, Ohigashi M, Osugi K, Yamakado K (2021) Clinical impact of 11C-Pittsburgh compound-B positron emission tomography in addition to magnetic resonance imaging and single-photon emission computed tomography on diagnosis of mild cognitive impairment to Alzheimers disease. *Medicine* 100(3):e23969
73. Martínez G, Vernooij RW, Padilla PF, Zamora J, Flicker L, Cosp XB (2017) 18F PET with flutemetamol for the early diagnosis of Alzheimers disease dementia and other dementias in people with mild cognitive impairment (MCI). *Cochrane Database Syst Rev*. <https://doi.org/10.1002/14651858.CD012884/full>
74. Ding Y, Sohn JH, Kawczynski MG, Trivedi H, Harnish R, Jenkins NW, Franc BL (2019) A deep learning model to predict a diagnosis of alzheimer disease by using 18F-FDG PET of the brain. *Radiology* 290(2):456–464
75. Zhang S, Han D, Tan X, Feng J, Guo Y, Ding Y (2012) Diagnostic accuracy of 18F-FDG and 11C-PIB-PET for prediction of short-term conversion to Alzheimer’s disease in subjects with mild cognitive impairment. *Int J Clin Pract* 66(2):185–198
76. Ma Y, Zhang S, Li J, Zheng D, Guo Y, Feng J, Ren W (2014) Predictive accuracy of amyloid imaging for progression from mild cognitive impairment to alzheimer disease with different lengths of follow-up. *Medicine* 93(27):e150
77. Peng J, Zhu X, Wang Y, An L, Shen D (2019) Structured sparsity regularized multiple kernel learning for Alzheimer’s disease diagnosis. *Pattern Recogn* 88:370–382

78. Suk H-I, Lee S-W, Shen D (2015) Latent feature representation with stacked auto-encoder for AD/MCI diagnosis. *Brain Struct Funct* 220(2):841–859
79. Zheng N, Qiu H, Wang Z, Liu W, Zhang H, Li Y (2018) A new switching-delayed-PSO-based optimized SVM algorithm for diagnosis of Alzheimer's Disease. *Neurocomputing* 320:195–202
80. Kim J, Lee B (2018) Identification of Alzheimers disease and mild cognitive impairment using multimodal sparse hierarchical extreme learning machine. *Hum Brain Mapp* 39(9):3728–3741
81. Chételat G, Arbizu J, Barthel H, Garibotto V, Law I, Morbelli S, Drzezga A (2020) Amyloid-PET and 18F-FDG-PET in the diagnostic investigation of Alzheimers disease and other dementias. *Lancet Neurol* 19(11):951–962
82. Suppiah S, Ching SM, Mfammed AJ, Mrad SV (2018) The role of PET/CT amyloid imaging compared with Tc99m-HMPAO SPECT imaging for diagnosing Alzheimer's. *Med J Malaysia* 73(3):147
83. Zhang D, Shen D (2012) Predicting future clinical changes of MCI patients using longitudinal and multimodal biomarkers. *PLoS ONE* 7(3):e33182
84. Suk H, Lee S, Shen D (2014) Hierarchical feature representation and multimodal fusion with deep learning for AD/MCI diagnosis. *Neuroimage* 101:569–582
85. Wang P, Chen K, Yao L, Hu B, Wu X, Zhang J, Guo X (2016) Multimodal classification of mild cognitive impairment based on partial least squares. *J Alzheimers Dis* 54(1):359–371
86. Devanand D, Mikhno A, Pelton GH, Cuasay K, Pradhavan G, Kumar JD, Parsey RV (2010) Pittsburgh compound B (11C-PIB) and fluorodeoxyglucose (18 F-FDG) PET in patients with alzheimer disease, mild cognitive impairment, and healthy controls. *J Geriatr Psychiatry Neurol* 23(3):185–198
87. Yang Z, Liu Z (2020) The risk prediction of Alzheimer's Disease based on the deep learning model of brain 18F-FDG positron emission tomography. *Saudi J Biol Sci* 27(2):659–665
88. Ortiz A, Munilla J, Górriz JM, Ramírez J (2016) Ensembles of deep learning architectures for the early diagnosis of the Alzheimer's disease. *Int J Neural Syst* 26(07):1650025
89. Vandenberghe R, Nelissen N, Salmon E, Ivanoiu A, Hasselbalch S, Andersen A, Dupont P (2013) Binary classification of 18F-flutemetamol PET using machine learning: comparison with visual reads and structural MRI. *Neuroimage* 64:517–525
90. Sivapriya TR, Kamal AR, Thangaiah PR (2015) Ensemble merit merge feature selection for enhanced multinomial classification in Alzheimer's Dementia. *Comput Math Methods Med* 2015:1–11
91. Cheng Bo, Liu M, Zhang D, Munsell BC, Shen D (2015) Domain transfer learning for MCI conversion prediction. *IEEE Trans Biomed Eng* 62(7):1805–1817
92. Mosconi L, McHugh PF (2011) FDG-and amyloid-PET in Alzheimer's Disease: Is the whole greater than the sum of the parts. *Q J Nucl Med Mol Imaging* 55(3):250
93. Rabinovici GD, Rosen HJ, Alkalay A, Kornak J, Furst AJ, Agarwal N, Jagust WJ (2011) Amyloid vs FDG-PET in the differential diagnosis of AD and FTL. *Neurology* 77(23):2034–2042
94. Tong T, Gray K, Gao Q, Chen L, Rueckert D (2017) Multi-modal classification of Alzheimer's disease using nonlinear graph fusion. *Pattern Recognit* 63:171–181. <https://doi.org/10.1016/j.patcog.2016.10.009>
95. Young J, Modat M, Cardoso MJ, Mendelson A, Cash D, Ourselin S (2013) Accurate multimodal probabilistic prediction of conversion to Alzheimer's Disease in patients with mild cognitive impairment. *NeuroImage Clin* 2:735–745. <https://doi.org/10.1016/j.nicl.2013.05.004>
96. Mora Moradi E, Pepe A, Gaser C, Huttunen H, Tohka J (2015) Machine learning framework for early MRI-based Alzheimers conversion prediction in MCI subjects. *Neuroimage* 104:398–412
97. Teng L, Li Y, Zhao Y, Hu T, Zhang Z, Yao Z, Hu B (2020) Predicting MCI progression with FDG-PET and cognitive scores: a longitudinal study. *BMC Neurol*. <https://doi.org/10.1186/s12883-020-01728-x>

Publisher's Note Springer Nature remains neutral with regard to jurisdictional claims in published maps and institutional affiliations.